crystals

MDPI

Article

Two-Dimensional Carbon Networks with a Negative Poisson's Ratio

Hao Yuan [1,2], Guan Huang [1,2], Guangzhao Qin [3], Lichuan Zhang [1,2,*], Yuee Xie [1,2,*] and Yuanping Chen [1,2,*]

[1] School of Physics and Electronic Engineering, Jiangsu University, Zhenjiang 212013, China
[2] Jiangsu Engineering Research Center on Quantum Perception and Intelligent Detection of Agricultural Information, Zhenjiang 212013, China
[3] State Key Laboratory of Advanced Design and Manufacturing for Vehicle Body, College of Mechanical and Vehicle Engineering, Hunan University, Changsha 410082, China
* Correspondence: lichuan.zhang@ujs.edu.cn (L.Z.); yueex@ujs.edu.cn (Y.X.); chenyp@ujs.edu.cn (Y.C.)

Abstract: Low-dimensional materials with a negative Poisson's ratio (NPR) have attracted lots of attention for their potential applications in aerospace, defense, etc. Although graphene and monolayer h-BN have been reported to have NPR behavior under external strains, the mechanism is not clear, and the critical strains of the occurrence of a NPR are relatively larger. Here, we propose that the origination of the NPR phenomena in the 2D honeycomb structures can be explained by the variation of the zigzag chains under strains. Our calculations clarify that a NPR occurs along the armchair-chain direction rather than the zigzag-chain direction in these materials. Furthermore, a series of two-dimensional carbon networks including zigzag chains have demonstrated that there is NPR phenomena in them. In some of the networks, a NPR can be found under a small external strain. Our study not only deepens the understanding of the origin of NPR in honeycomb systems but also offers guidance to design auxetic nanostructures.

Keywords: honeycomb lattice; carbon allotropes; negative Poisson's ratio; mechanical properties; two-dimensional material

Citation: Yuan, H.; Huang, G.; Qin, G.; Zhang, L.; Xie, Y.; Chen, Y. Two-Dimensional Carbon Networks with a Negative Poisson's Ratio. *Crystals* **2023**, *13*, 442. https://doi.org/10.3390/cryst13030442

Academic Editors: Pingheng Tan and Igor Neri

Received: 25 November 2022
Revised: 2 February 2023
Accepted: 1 March 2023
Published: 3 March 2023

1. Introduction

The Poisson's ratio, i.e., the ratio between the lateral and longitudinal strain for the stretched material, is an important parameter to describe the physical and mechanical properties of materials. In contrast to conventional materials, the materials with a negative Poisson's ratio (NPR) (also called auxetic materials) [1] possess some exotic physical properties [2–4], such as high specific strength [5,6], high energy absorption [7], enhanced shear resistance [8,9], indentation resistance [10,11], and fracture toughness [12]. These remarkable properties motivate researchers to search for various NPR materials [13–23]. So far, the NPR phenomenon has been discovered in many three-dimensional (3D) structures, such as some metallic cubic structures [24,25] and some structures constructed by beams [26,27] or rigid units [28]. In addition, some artificial 3D auxetic materials have also been reported [29,30].

In recent years, the NPR phenomenon has been found in some two-dimensional (2D) materials, including buckled structures [30–37], such as 2D silica [31], penta-B_2N_4 [32], δ-SnS [33], penta-SiCN [34], penta-Be_5C_2 [35], penta-graphene [36], SiS [37], δ-Phosphorene [38] and some planar honeycomb materials [39–45], such as graphene [39–42], h-BN [43], and h-GaN [44]. Although a lot of calculations have been carried out for these 2D planar materials, the mechanism of the NPR in them is still unclear. Another issue is that, in some materials, e.g., graphene, in order to generate the NPR phenomenon, a larger critical strain is required. According to the calculations of molecular dynamics (MD) [39] and density functional theory (DFT) [40,41], 6% and 18% uniaxial strain along the armchair-chain direction in graphene are needed, respectively [46,47]. A larger strain is

not easy to be realized in application. Therefore, it is natural to ask, can we find a physical mechanism for the NPR phenomenon in the 2D materials; furthermore, can we find some 2D carbon networks possessing lower critical strains than graphene?

In this paper, we find that the NPR phenomenon in 2D carbon materials [48] could originate from the zigzag chains. We first study the mechanical response of a zigzag carbon chain, and the NPR phenomenon is found. Then, we construct some 2D planar carbon structures including zigzag chains. The NPR phenomena have been observed in them when strains along the vertical direction of the zigzag chains are applied. Moreover, several 2D carbon structures have smaller critical strains than graphene. As a comparison, some 2D carbon structures with no zigzag chains have also been constructed, and no NPR is found in them. Our study deepens the understanding of the origins of a NPR in 2D materials, which would shed light on the advanced design of nanoscale electromechanical devices.

2. Materials and Methods

The calculations are mainly performed based on the classical MD method [49,50] to investigate the strain response of different materials, and the Lammps program with the Airebo potential function [51] is used for the simulation. During the MD simulation, the Airebo potential function is selected to describe the C-C interaction, which is widely used to study the mechanical properties and strain effects of carbon materials. In the calculations of the mechanical response, the relaxation of 50,000 steps is performed for the structure with temperature 10 K. The time step is selected as 1 fs, which is small enough to maintain energy conservation during the MD simulation. To verify that the Airebo potential function is appropriate, the Lammps package, together with the Airebo potential function, is adopted to stretch the y-axis (armchair) of graphene, and the obtained results are consistent with the previous study [41].

To verify the stability of the structures, the first-principle theory with the projector augmented wave (PAW) method [52] implemented in the Vienna ab initio Simulation Package (VASP) [53] is selected for the calculation. The electron exchange-correlation is described with the generalized gradient approximation (GGA) [54] of Perdew-Burke -Ernzerhof (PBE) [55], and the Monkhorst-Pack k-mesh [56] of $15 \times 15 \times 1$ is employed to sample the irreducible Brillouin zone. The kinetic energy cutoff for the plane wave functions is set to 450 eV and the energy convergence threshold is chosen as 10^{-8} eV to ensure calculational accuracy. All of the atomic positions and lattice structures are completely relaxed, and the maximum force threshold is 0.02 eV/Å. In the calculation of the phonon spectrum, the structure is expanded by $4 \times 4 \times 1$. The structure is processed by the phonopy program [57] and the phonon spectrum is calculated with the finite displacement method. The 20 Å vacuum layer is chosen to eliminate the interaction between different layers.

To explore the properties of NPR, the ε_x and ε_y are introduced to indicate the relative strain along the x- and y-axis, respectively, and the ε_i ($i \in (x, y)$) is defined as $\varepsilon_i = \left(L_i - L_{i_0}\right)/L_{i_0}$, where L_{i_0} and L_i are the initial and deformation lengths of the unit cell along the i-axis ($i \in (x, y)$). Then, the Poisson's ratio can be defined as $v = -\partial\varepsilon_x/\partial\varepsilon_y$ [58]. One thing we would like to emphasize is that in some previous works, the Poisson's ratio is defined as $v = -\varepsilon_x/\varepsilon_y$ [2,4,41,59]. With the latter definition, until the failure of the structure, no NPR occurs in graphene [2], which is not adopted in this work.

3. Results

3.1. Mechanical Properties of a Zigzag Carbon Chain

Graphene can be regarded as a combination of zigzag carbon chains (illustrated in Figure S1), so it is meaningful to study the mechanical response of the zigzag chain to explain the mechanical properties of graphene. To ensure the coordination number of the studied carbon atoms is 3 in the zigzag carbon chain, the structure of the zigzag carbon chain is chosen, as shown in Figure 1a. The blue dotted box represents the unit cell of the zigzag carbon chain, and the 20 Å vacuum layers are applied in the y- and z-axis. In Figure 1a, the bond angle, bond length, and lattice constant are marked by d, θ and a, respectively,

where the optimized lattice constants are $a = 2.285$Å, $d = 1.42$Å, and $\theta = 115.82°$. To investigate the mechanical response of the zigzag carbon chain, it is expanded 40 unit cells along the x-axis, and the strain is applied along the y-axis. To simulate the zigzag chain under a vertical compressive or tensile strain, the upper and lower brown carbon atoms (in the black dotted boxes) are shifted toward or backward to the red atoms, respectively, and then they are fixed. The Lammps program with the Airebo potential function is used to simulate the mechanical response of the red atoms in the zigzag chain.

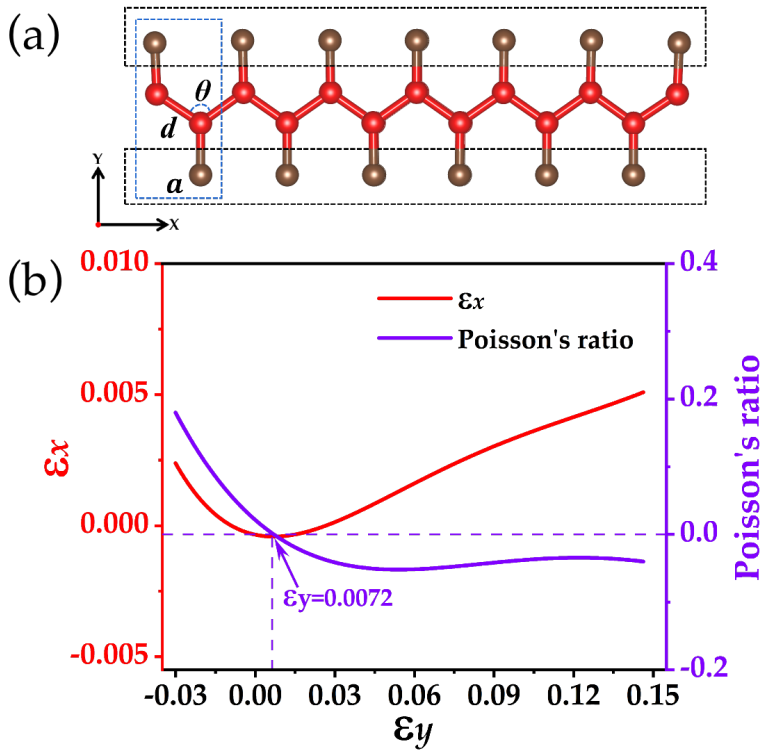

Figure 1. The schematic structure of the optimized zigzag carbon chain in (**a**) and the mechanical response under the uniaxial strain along y-axis in (**b**). The bond angle and the bond length are marked by d and θ. The fixed carbon atoms are represented by the brown balls and the red balls are free-moving carbon atoms. ε_y is the strain along the y-axis, and ε_x is the response of the driven strain in the x-axis. The red line indicates the $\varepsilon_x - \varepsilon_y$ curve under the uniaxial strain along the y direction, and the purple line represents Poisson's ratio under the uniaxial strain along the y-axis. The purple dotted line represents zero Poisson's ratio.

The mechanical response of the zigzag chain is shown in Figure 1b, in which the red line indicates the variation of the lengths of the unit cell under a strain along y-axis. It is found that a turning point appears in the case of $\varepsilon_y = 0.007$ with the structure parameters $d = 1.421$ Å and $\theta = 115.82°$. The purple line is the Poisson's ratio curve. One can see that a NPR appears when $\varepsilon_y > 0.007$. The whole evolution of the carbon chain under stretch is available in the Supplementary Materials.

To explore the mechanical mechanism of the NPR phenomenon, we investigate the relation between the bond length, bond angle, and structural energy of the zigzag chain, shown in Figure 1a. Figure 2a presents the zigzag chain extracted from Figure 1a. The distance of two next-nearest atoms is labeled as x, and the thickness of the zigzag chain is labeled as y. The bond angle is labeled as θ. The black dots represent the intrinsic zigzag chain without strain. The optimized parameters of the intrinsic zigzag chain is $x_0 = 2.40$ Å, $y_0 = 0.75$ Å, $\theta_0 = 115.82°$. When tensile strain is applied on the zigzag chain along the y-axis, the atoms in the zigzag chain shift away from the equilibrium positions, as shown by the red dots in Figure 2a. With the increase in y, i.e., $\Delta y = y - y_0 > 0$ ($\varepsilon_y > 0$), if $\Delta x = x - x_0 > 0$ ($\varepsilon_x > 0$), a NPR occurs. Otherwise, the Poisson's ratio is positive.

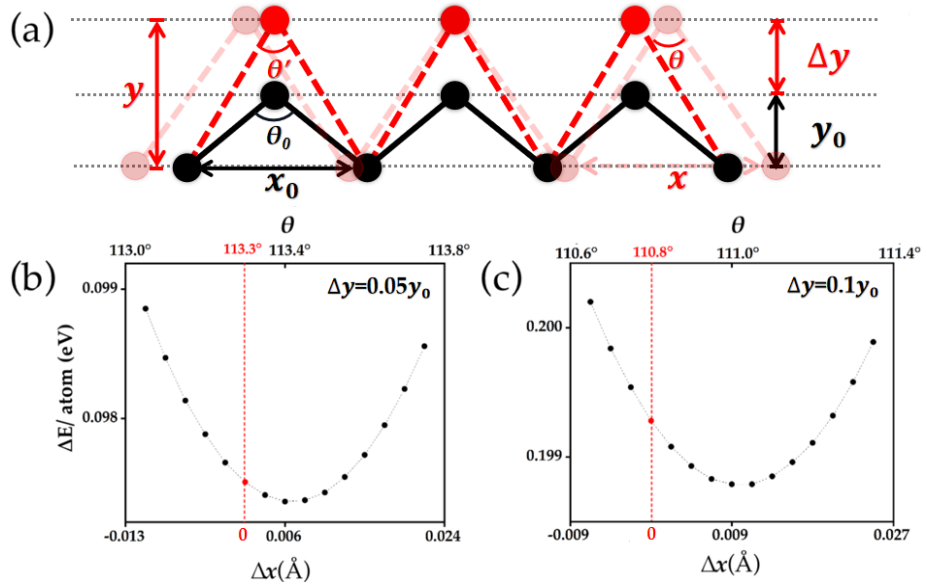

Figure 2. (**a**) A schematic view of a zigzag chain under a tensile strain. The black dots represent an intrinsic zigzag chain without strain, determined by structure parameters θ_0, x_0 and y_0. The light red dots represent the final chain under a tensile strain along $y-$axis, where structure parameters change from y_0 to y and θ_0 to θ. Here, the red dots correspond to the case that y_0 changes into y and $\Delta x = 0$. (**b**,**c**) The change of energy (per carbon atom) for the zigzag chain as a function of $\Delta x = x' - x_0$ is shown in (**b**,**c**) with tensile strain $\Delta y = 0.05y_0$ (**b**) and $\Delta y = 0.1y_0$ (**c**), separately. Following Equation (1), the variation of angle θ corresponds to the variation of Δx.

In Figure 2b,c, we calculate the ΔE/atom of the zigzag chain as a function of Δx, when $\Delta y = 0.05y_0$ and $\Delta y = 0.1y_0$. Here, ΔE refers to the difference in the energy between the changed structure and the initial structure (the relaxed structure without any strain). The variation of Δx is also related to the variation of the bond angle θ. The relation between the structural parameters is:

$$\Delta x = x - x_0 = 2y\left(\tan\frac{\theta}{2} - \tan\frac{\theta'}{2}\right) \quad (1)$$

where the angle θ' refers to the hypothetical situation that $\Delta x = 0$ and $\Delta y > 0$. Seen from Figure 2b, when $\Delta y = 0.05\ y_0$, the lowest energy occurs at Δx = 0.006Å. This means that the bond angle θ is larger than θ' and the zigzag chain needs to be extended to reduce the total energy. Figure 2c presents the relation between Δy and Δx when a tensile strain is applied along the y-axis with $\Delta y = 0.1y_0$. One can obtain a conclusion similar to the case in Figure 2b, i.e., a tensile strain along the vertical direction of the zigzag chain will extend the chain.

It is noted that the bond angle θ of the intrinsic zigzag chain is 115.82°, while the bond angle in graphene is 120°. Graphene is the most sTable 2D carbon allotrope, which indicates that in a 2D carbon structure, a smaller angle will increase the structural energy. To reduce the total energy of the structure, the bond angle will increase. This is the reason that a zigzag chain extends along the chain direction when a vertical tensile strain shrinks the bond angle.

3.2. NPR in Some 2D Carbon Networks

It is demonstrated above that a zigzag carbon chain holds a NPR phenomenon when a tensile strain is applied perpendicular to the chain. Next, we sought to investigate whether the zigzag chain plays an important role in the occurrence of NPR in 2D carbon materials. To answer this question, except for graphene, three types of 2D planar carbon materials, constructed by zigzag carbon chains, are chosen to investigate the mechanical response. The

schematic structures of these three materials are shown in Figure 3a,c,e, and the proportion of the zigzag carbon chains (marked by red color) in these structures are 66.67%, 80%, and 57.14%, respectively.

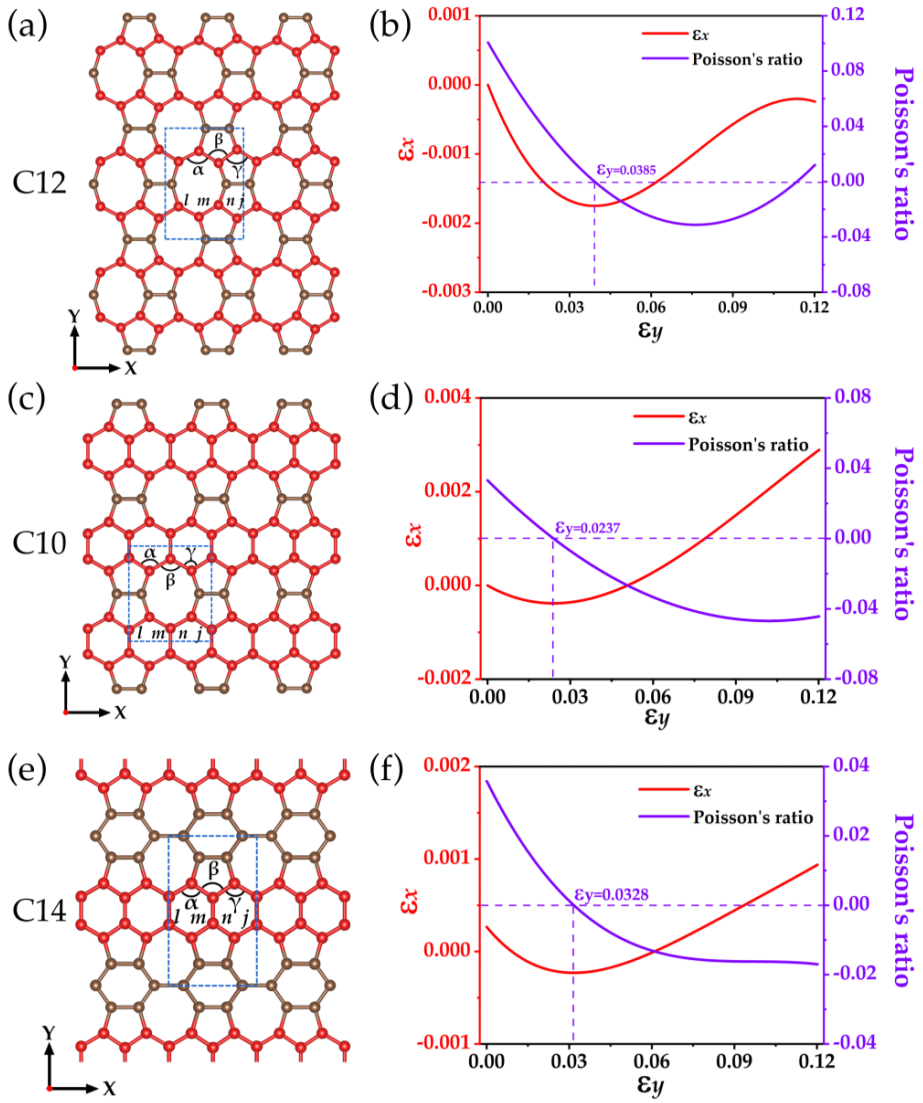

Figure 3. Structures and mechanical responses of C12, C10, and C14. (**a**,**c**,**e**) Three structures containing zigzag carbon chains are marked as C12, C10, and C14, separately. The bond angle and the bond length of these structures are marked with α, β, γ and l, m, n, j, respectively. The unit cell in these structures is outlined with blue rectangular dotted boxes, and zigzag chains in these structures are colored red. The mechanical responses for structures (**a**,**c**,**e**) are shown in (**b**,**d**,**f**), separately. These red lines indicate the response of the driven strain under the uniaxial strain along the y-axis, and the purple line represents the Poisson's ratio under the uniaxial strain along the y-axis.

The stability of these materials is verified by the calculated phonon dispersion based on the DFT calculation, which shows that there is no imaginary frequency (see Figure S2 in the Supplementary Materials). Among three structures, the C12, also called OPG-Z, has already been discovered by Su et al. [60]. Based on the MD simulation carried out by Lammps, the $\varepsilon_x - \varepsilon_y$ curve (red line) and the Poisson's ratio curve (purple line) are plotted in Figure 3b,d,f. These red and purple lines indicate that a NPR occurs when ε_y is equal to 3.85%, 2.37%, and 3.28%. It is demonstrated that under a strain along the y-axis, C10 is the first one to incur a NPR, which has the highest proportion of zigzag chains; while C14 is the last one to show a NPR, which has the lowest proportion of zigzag chains. Moreover,

by comparing the bond lengths and bond angles of the carbon chains in these materials, we found that these chains are similar to those in Figure 1 (more details can be found in Tables S1 and S2 in the Supplementary Materials). These results generate a hypothesis that the proportion of carbon chains has a positive correlation with the occurrence of a NPR.

To verify this hypothesis, more than 600 structures are searched according to our structure search program of 2D carbon materials [61]. In addition to these carbon structures, shown in Figure 3, three sTable 2D carbon structures, C36, C20, and C24, are obtained (the phonon dispersion is shown in Figure S2 of the Supplementary Materials). The percentage of zigzag chains (marked by red color) in C36, C20 and C24 are 44.44%, 40% and 33.33%, respectively. We have carried out MD simulations on these structures and investigated the mechanical response, as shown in Figure 4. In these three materials, a NPR occurs when the values of ε_y are 9.725%, 11.548%, and 13.31%, which is consistent with our hypothesis.

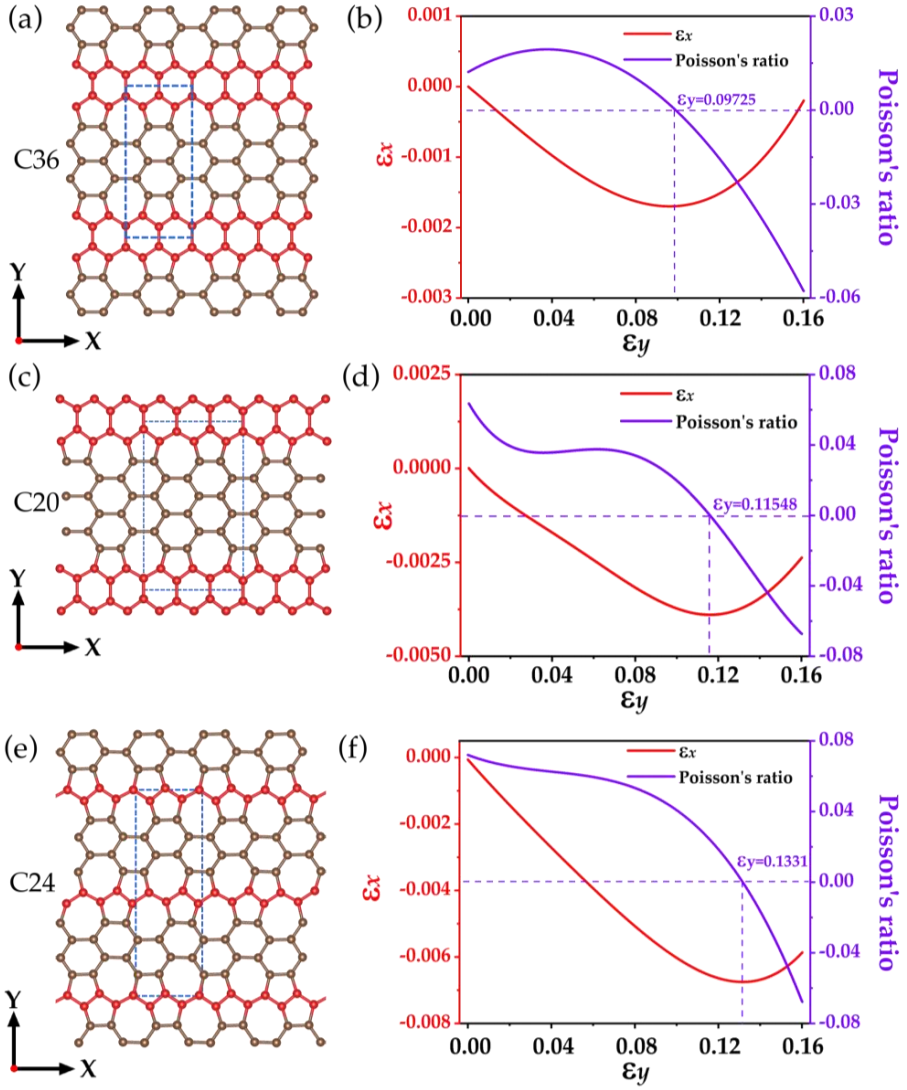

Figure 4. Structure and mechanical properties of C36, C20, and C24 (**a**,**c**,**e**). Three structures containing zigzag carbon chains are marked as C36, C20, and C24, separately. The mechanical responses of structures (**a**,**c**,**e**) are shown in (**b**,**d**,**f**), separately. The red line indicates the response of the driven strain under the uniaxial strain along the *y*-axis, and the purple line represents the Poisson's ratio under the uniaxial strain along the *y*-axis.

Moreover, as shown in Figure 5, two carbon networks without zigzag carbon chains, marked as C16 and C32, are chosen to compare the mechanical response under strain. The phonon dispersions of C16 and C32 are shown in Figure S2 of the supplementary materials.

It is clear that the zigzag carbon chain is absent in both the *x*- and *y*-axis. The mechanical response of these two structures is studied when the uniaxial stretch is applied in both the *x*- and *y*-axis. As shown in Figure 5c–f, until the structure arrives at mechanical failure, there is no NPR. To return to the structures discussed in Figures 3 and 4, there is no zigzag chain perpendicular to the *x*-axis. The Poisson's ratios of these structures along the *x*-axis are calculated and no NPR occurs, as shown in Figure S3 of the Supplementary Materials. Thus, we conclude that the zigzag carbon chain plays a crucial role in the mechanical properties of 2D carbon materials, and it has a positive effect on the occurrence of NPR. The simulation is processed by the MD method with the Airebo function, and the calculated Poisson's ratio may be difference under other methods, e.g., DFT [46,47]. However, as shown in Figure S5, these quantitative differences do not influence the qualitative results.

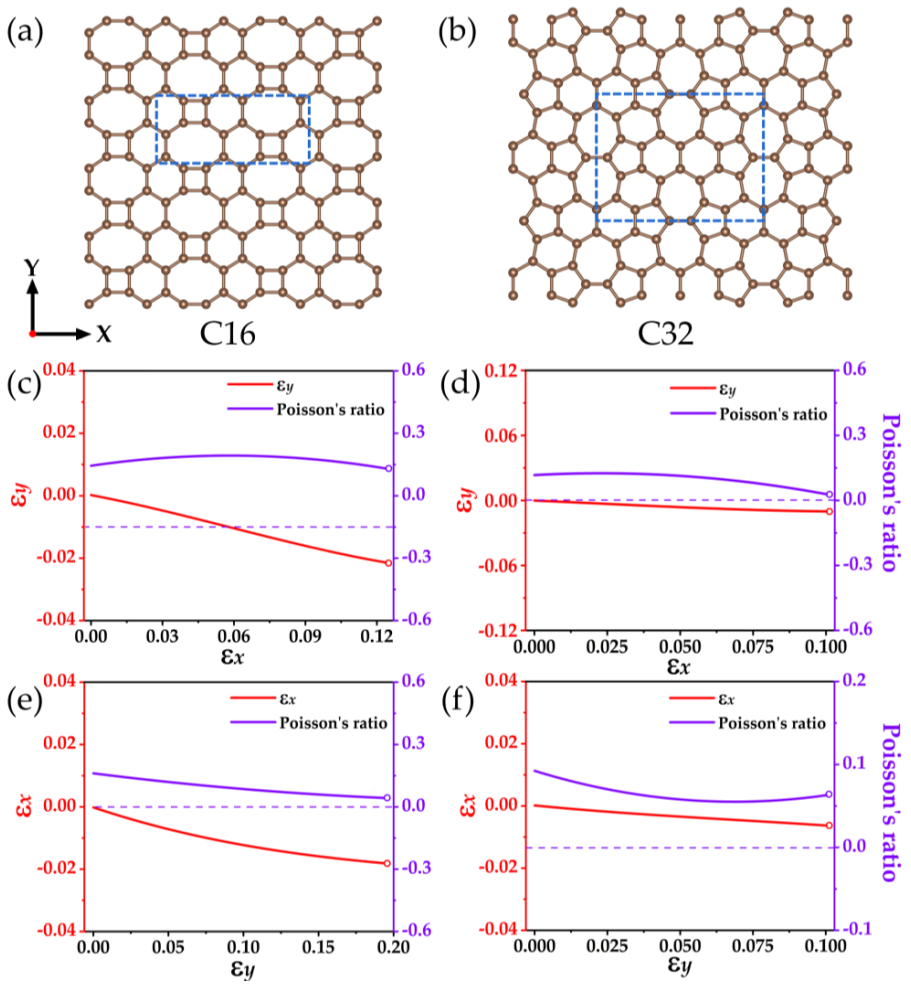

Figure 5. Structures and mechanical properties of C16 and C32. Two structures of C16 and C32 are shown in (**a**,**b**). The mechanical responses of C16 and C32 are shown in (**c**,**e**) and (**d**,**f**). Red lines represent the response of the driven strain under the uniaxial strain along the *x*- and *y*-axis, respectively, and purple lines represent the Poisson's ratio under the uniaxial strain along the *x*- and *y*-axis, respectively.

The Poisson's ratio is not only determined by the direction, but is also influenced by the temperature. The structure C10 is chosen to test the influence of the temperature, and more details are shown in the supplementary material. It is noted that the mechanism of a NPR in our work is different from the occurrence of a NPR in vacancy-defected graphene structures [39], whose NPR is aroused by the rippled structure.

4. Conclusions

In summary, we investigate the mechanical response of some 2D planar carbon networks. First, the NPR in the zigzag carbon chain is uncovered. We found that the zigzag carbon chain has a strong relationship with the occurrence of a NPR. Some 2D planar carbon structures, including zigzag chains, indeed possess NPR phenomena when strains are applied along the vertical direction of the zigzag chains in the structures. Several 2D carbon structures have smaller critical strains to obtain a NPR compared with graphene. In contrast, the carbon structures with no zigzag chains were not found to have a NPR in the structures. Our study can not only be used to explain the occurrence of a NPR in 2D carbon structures, but can also be extended to explain a NPR in all 2D honeycomb systems or 2D structures, including zigzag chains.

Supplementary Materials: The following supporting information can be downloaded at: https://www.mdpi.com/article/10.3390/cryst13030442/s1. Figure S1. (a) The schematic structure of graphene. Here, the zigzag chain is marked with two different colors. (b)The mechanical response of graphene. the red line indicates the ε_x–ε_y curve under the uniaxial strain along the y-direction, and the purple line represents Poisson's ratio under the uniaxial strain along the y direction. The purple dotted line represents the zero Poisson's ratio. Figure S2. The phonon dispersion of four structures C12, C16, C10, and C32. The Brillouin zone of these four structures is rectangular, and the phonon dispersion profile show positive values along G-X-S-Y-G. The phonon dispersion of four structures C20, C14, C24, and C36. The Brillouin zone of these four structures is rectangular, and the phonon dispersion profile show positive values along G-X-S-Y-G-S. Figure S3. The mechanical response of C12, C10, C14, C36, C20, C24 under the uniaxial strain along the x-axis. The red line indicates the response of the driven strain under the uniaxial strain along the x-axis, and the purple line represents the Poisson's ratio under the uniaxial strain along the y direction. The purple dashed line indicating the zero Poisson's ratio state. Figure S4. Poisson's ratio curves and strain curves of C10, at the temperature of 300 K and 10 K. Figure S5. The result of mechanical responses of structures graphene, C10, and C16 according to DFT calculations. The red line indicates the response of the driven strain under the uniaxial strain along the y-axis, and the purple line represents Poisson's ratio under the uniaxial strain along the y-axis. Table S1. Structure parameters of C12, C10, and C14 with the initial case; the case for the appearance of NPR, and the case when 11% stretch is applied. Bond angles and bond lengths of these structures are marked with α, β, γ and l, m, n, j in Figure 3 of the manuscript. Table S2. The average bond lengths and bond angles for structures C12, C10, C14, C36, C20, and C24, and no external strain is applied. Table S3. The effective elastic constants of C10, C12, C14, and graphene according to the MD with Airebo function and DFT calculations.

Author Contributions: H.Y.: Conceptualization, Methodology, Software, Investigation, Formal analysis, Writing—original draft. G.H.: Data curation, Investigation, Writing—original draft. L.Z.: Supervision, Writing—review and editing. G.Q.: Discussion, Modifying original draft. Y.C. and Y.X.: Conceptualization, Funding acquisition, Resources, Supervision. All authors have read and agreed to the published version of the manuscript.

Funding: This work gratefully acknowledges the financial support of the National Natural Science Foundation of China (No. 12174157, 12074150, 12174158 and 11874314). G. Qin acknowledges the support of the Natural Science Foundation of Chongqing, China (No. CSTB2022 NSCQ-MSX0332).

Data Availability Statement: Data available on reasonable request.

Acknowledgments: We thank Muhammad Idrees for their helpful discussions.

Conflicts of Interest: The authors declare that they have no known competing financial interests or personal relationships that could have appeared to influence the work reported in this paper.

References

1. Huang, C.; Chen, L. Negative Poisson's ratio in modern functional materials. *Adv. Mater.* **2016**, *28*, 8079–8096. [CrossRef] [PubMed]
2. Liu, F.; Ming, P.B.; Li, J. Ab initio calculation of ideal strength and phonon instability of graphene under tension. *Phys. Rev. B* **2007**, *76*, 064120. [CrossRef]

3. Zeinalipour-Yazdi, C.D.; Christofides, C. Linear correlation between binding energy and Young's modulus in graphene nanoribbons. *J. Appl. Phys.* **2009**, *106*, 054318. [CrossRef]
4. Kalosakas, G.; Lathiotakis, N.N.; Galiotis, C.; Papagelis, K. In-plane force fields and elastic properties of graphene. *J. Appl. Phys.* **2013**, *113*, 134307. [CrossRef]
5. Fu, M.H.; Xu, O.T.; Hu, L.L.; Yu, T.X. Nonlinear shear modulus of re-entrant hexagonal honeycombs under large deformation. *Int. J. Solids. Struct.* **2016**, *80*, 284–296. [CrossRef]
6. Zhong, R.; Fu, M.; Yin, Q.; Xu, O.; Hu, L. Special characteristics of tetrachiral honeycombs under large deformation. *Int. J. Solids. Struct.* **2019**, *169*, 166–176. [CrossRef]
7. Zhou, G.; Zhao, W.; Li, Q.; Shen, W.; Wang, C. Multi-objective robust design optimization of a novel NPR energy absorption structure for vehicles front ends to enhance pedestrian lower leg protection. *Struct. Multidiscip. Optim.* **2017**, *56*, 1215–1224. [CrossRef]
8. Li, Z.; Gu, Y.; He, C.; Zou, X. Fully auxetic and multifunctional of two-dimensional δ-GeS and δ-GeSe. *Phys. Rev. B* **2022**, *106*, 035426. [CrossRef]
9. Zhao, S.; Zhang, Y.; Zhang, Y.; Yang, J.; Kitipornchai, S. Graphene origami-enabled auxetic metallic metamaterials: An atomistic insight. *Int. J. Mech. Sci.* **2021**, *212*, 106814. [CrossRef]
10. Li, Z.; Wang, K.F.; Wang, B.L. Indentation resistance of brittle auxetic structures: Combining discrete representation and continuum model. *Eng. Fract. Mech.* **2021**, *252*, 107824. [CrossRef]
11. Hu, L.L.; Zhou, M.Z.; Deng, H. Dynamic indentation of auxetic and non-auxetic honeycombs under large deformation. *Compos. Struct.* **2019**, *207*, 323–330. [CrossRef]
12. Fernando, P.L. Fracture toughness of filled polypropylene copolymer systems. *Polym. Eng. Sci.* **1988**, *28*, 806–814. [CrossRef]
13. Gorodtsov, V.A.; Lisovenko, D.S. The Extreme Values of Young's Modulus and the Negative Poisson's Ratios of Rhombic Crystals. *Crystals* **2021**, *11*, 863. [CrossRef]
14. Zhou, Y.; Zhou, C.; Shu, Z.; Jia, L.J. Effect of two-dimensional re-entrant honeycomb configuration on elastoplastic performance of perforated steel plate. *Appl. Sci.* **2020**, *10*, 3067. [CrossRef]
15. Ghavidelnia, N.; Bodaghi, M.; Hedayati, R. Idealized 3D auxetic mechanical metamaterial: An analytical, numerical, and experimental study. *Materials* **2021**, *14*, 993. [CrossRef]
16. Liu, B.; Niu, M.; Fu, J.; Xi, Z.; Lei, M.; Quhe, R. Negative Poisson's ratio in puckered two-dimensional materials. *Phys. Rev. Mater.* **2019**, *3*, 054002. [CrossRef]
17. La Malfa, F.; Puce, S.; Rizzi, F.; De Vittorio, M. A flexible carbon nanotubes-based auxetic sponge electrode for strain sensors. *Nanomater.* **2020**, *10*, 2365. [CrossRef]
18. Wojciechowski, K.W. Constant thermodynamic tension Monte Carlo studies of elastic properties of a two- dimensional system of hard cyclic hexamers. *Mol. Phys.* **1987**, *61*, 1247–1258. [CrossRef]
19. Shlomo, S. Energy level density of nuclei. *Nucl. Phys. A* **1992**, *539*, 17–36. [CrossRef]
20. Scarpa, F.; Narojczyk, J.W.; Wojciechowski, K.W. Unusual deformation mechanisms in carbon nanotube hetero junctions (5, 5)–(10, 10) under tensile loading. *Phys. Status. Solidi. B* **2011**, *248*, 82–87. [CrossRef]
21. Lvov, V.A.; Senatov, F.S.; Veveris, A.A.; Skrybykina, V.A.; Díaz Lantada, A. Auxetic Metamaterials for Biomedical Devices: Current Situation, Main Chall -enges, and Research Trends. *Materials* **2022**, *15*, 1439. [CrossRef] [PubMed]
22. Bilski, M.; Pigłowski, P.M.; Wojciechowski, K.W. Extreme Poisson's ratios of honeycomb, re-entrant, and zig-zag crystals of binary hard discs. *Symmetry* **2021**, *13*, 1127. [CrossRef]
23. Bilski, M.; Wojciechowski, K.W.; Stręk, T.; Kędziora, P.; Grima-Cornish, J.N.; Dudek, M.R. Extremely non-auxetic behavior of a typical auxetic microstructure due to its material properties. *Materials* **2021**, *14*, 7837. [CrossRef] [PubMed]
24. Lv, W.; Li, D.; Dong, L. Study on blast resistance of a composite sandwich panel with isotropic foam core with negative Poisson's ratio. *Int. J. Mech. Sci.* **2021**, *191*, 106105. [CrossRef]
25. Baughman, R.H.; Shacklette, J.M.; Zakhidov, A.A.; Stafström, S. Negative Poisson's ratios as a common feature of cubic metals. *Nature* **1998**, *392*, 362–365. [CrossRef]
26. Hughes, T.P.; Marmier, A.; Evans, K.E. Auxetic frameworks inspired by cubic crystals. *Int. J. Solids. Struct.* **2010**, *47*, 1469–1476. [CrossRef]
27. Pikhitsa, P.V.; Choi, M.; Kim, H.J.; Ahn, S.H. Auxetic lattice of multipods. *Phys. Status. Solidi. B* **2009**, *246*, 2098–2101. [CrossRef]
28. Grima-Cornish, J.N.; Grima, J.N.; Attard, D. A novel mechanical metamaterial exhibiting auxetic behavior and negative compressibility. *Materials* **2019**, *13*, 79. [CrossRef]
29. Narojczyk, J.W.; Bilski, M.; Grima, J.N.; Kędziora, P.; Morozow, D.; Rucki, M.; Wojciechowski, K.W. Removing Auxetic Properties in fcc Hard Sphere Crystals by Orthogonal Nanochannels with Hard Spheres of Another Diameter. *Materials* **2022**, *15*, 1134. [CrossRef]
30. Lakes, R. Foam structures with a negative Poisson's ratio. *Science* **1987**, *235*, 1038–1040. [CrossRef]
31. Gao, Z.; Dong, X.; Li, N.; Ren, J. Novel two-dimensional silicon dioxide with in-plane negative Poisson's ratio. *Nano Lett.* **2017**, *17*, 772–777. [CrossRef] [PubMed]
32. Pang, Q.; Liu, L.; Zhao, J. Mechanical anisotropy and strain-tailored band structures of pentagonal boron nitride monolayers. *J. Appl. Phys.* **2017**, *122*, 094302. [CrossRef]

33. Zhang, Q.; Wang, X.; Yang, S. δ-SnS: An emerging bidirectional auxetic direct semiconductor with desirable carrier mobility and high-performance catalytic behavior toward the water-splitting reaction. *ACS Appl. Mater. Inter.* **2021**, *13*, 31934–31946. [CrossRef] [PubMed]
34. Sharma, S.B.; Qattan, I.A.; Jaishi, M.; Paudyal, D. Penta-SiCN: A Highly Auxetic Monolayer. *ACS Appl. Electron. Ma.* **2022**, *4*, 2561–2569. [CrossRef]
35. Wang, Y.; Li, F.; Li, Y.; Chen, Z. Semi-metallic Be5C2 monolayer global minimum with quasi-planar pentacoordinate carbons and negative Poisson's ratio. *Nat. Commun.* **2016**, *7*, 11488. [CrossRef]
36. Zhang, S.; Zhou, J.; Wang, Q.; Chen, X.; Kawazoe, Y.; Jena, P. Penta-graphene: A new carbon allotrope. *Proc. Natl. Acad. Sci. USA* **2015**, *7*, 191–207.
37. Jing, T.; Liang, D.; Deng, M.; Cai, S. Two-dimensional IV–VI materials with in-plane negative Poisson's ratio and anisotropic carrier mobility. *J. Mater. Chem. C* **2020**, *8*, 10382–10389. [CrossRef]
38. Wang, H.; Li, X.; Li, P.; Yang, J. δ-Phosphorene: A two dimensional material with a highly negative Poisson's ratio. *Nanoscale* **2017**, *9*, 850–855. [CrossRef]
39. Grima, J.N.; Winczewski, S.; Mizzi, L.; Grech, M.C.; Cauchi, R.; Gatt, R.; Rybicki, J. Tailoring graphene to achieve negative Poisson's ratio properties. *Adv. Mater.* **2015**, *27*, 1455–1459. [CrossRef]
40. Li, X.; Huang, C.; Hu, S.; Deng, B.; Chen, Z.; Han, W.; Chen, L. Negative and near-zero Poisson's ratios in 2D graphene/MoS_2 and graphene/h-BN heterostructures. *J. Mater. Chem. C* **2020**, *8*, 4021–4029. [CrossRef]
41. Xu, M.; Paci, J.T.; Oswald, J.; Belytschko, T. A constitutive equation for graphene based on density functional theory. *Int. J. Solids Struct.* **2012**, *49*, 2582–2589. [CrossRef]
42. Fan, Y.; Xiang, Y.; Shen, H.S. Temperature-dependent negative Poisson's ratio of monolayer graphene: Prediction from molecu lar dynamics simulations. *Nanotechnol. Rev.* **2019**, *8*, 415–421. [CrossRef]
43. Los, J.H.; Kroes, J.M.H.; Albe, K.; Gordillo, R.M.; Katsnelson, M.I.; Fasolino, A. Extended Tersoff potential for boron nitride: Energetics and elastic properties of pristine and defective h-BN. *Phys. Rev. B* **2017**, *96*, 184108. [CrossRef]
44. Peng, Q.; Liang, C.; Ji, W.; De, S. Mechanical properties of g-GaN: A first principles study. *Appl. Phys. A* **2013**, *113*, 483–490. [CrossRef]
45. Qin, G.; Qin, Z. Negative Poisson's ratio in two-dimensional honeycomb structures. *Npj. Comput. Mater.* **2020**, *6*, 51. [CrossRef]
46. Jiang, J.W.; Chang, T.; Guo, X.; Park, H.S. Intrinsic negative Poisson's ratio for single-layer graphene. *Nano Lett.* **2016**, *16*, 5286–5290. [CrossRef]
47. Qin, Z.; Qin, G.; Hu, M. Origin of anisotropic negative Poisson's ratio in graphene. *Nanoscale* **2018**, *10*, 10365–10370. [CrossRef]
48. Xu, M.; Liang, T.; Shi, M.; Chen, H. Graphene-like two-dimensional materials. *Chem. Rev.* **2013**, *113*, 3766–3798. [CrossRef]
49. Plimpton, S. Fast parallel algorithms for short-range molecular dynamics. *J. Comput. Phys.* **1995**, *117*, 1–19. [CrossRef]
50. Deng, B.; Hou, J.; Zhu, H.; Liu, S.; Liu, E.; Shi, Y.; Peng, Q. The normal-auxeticity mechanical phase transition in graphene. *2D Mater.* **2017**, *4*, 021020. [CrossRef]
51. Stuart, S.J.; Tutein, A.B.; Harrison, J.A. A reactive potential for hydrocarbons with intermolecular interactions. *J. Chem. Phys.* **2000**, *112*, 6472–6486. [CrossRef]
52. Blöchl, P.E. Projector augmented-wave method. *Phys. Rev. B* **1994**, *50*, 17953. [CrossRef]
53. Hafner, J. Ab-initio simulations of materials using VASP: Density-functional theory and beyond. *J. Comput. Chem.* **2008**, *29*, 2044–2078. [CrossRef]
54. Grimme, S. Semiempirical GGA-type density functional constructed with a long-range dispersion correction. *J. Comput. Chem.* **2006**, *27*, 1787–1799. [CrossRef]
55. Ernzerhof, M.; Scuseria, G.E. Assessment of the Perdew–Burke–Ernzerhof exchange-correlation functional. *J. Chem. Phys.* **1999**, *110*, 5029–5036. [CrossRef]
56. Rajagopal, G.; Needs, R.J.; Kenny, S.; Foulkes, W.M.C.; James, A. Quantum Monte Carlo calculations for solids using special k points methods. *Phys. Rev. Lett.* **1994**, *73*, 1959. [CrossRef]
57. Togo, A.; Tanaka, I. First principles phonon calculations in materials science. *Scripta. Mater.* **2015**, *108*, 1–5. [CrossRef]
58. Ho, D.T.; Park, S.D.; Kwon, S.Y.; Park, K.; Kim, S.Y. Negative Poisson's ratios in metal nanoplates. *Nat. Commun.* **2014**, *5*, 3255. [CrossRef] [PubMed]
59. Zhao, H.; Min, K.; Aluru, N.R. Size and chirality dependent elastic properties of graphene nanoribbons under uniaxial tension. *Nano Lett.* **2009**, *9*, 3012–3015. [CrossRef] [PubMed]
60. Su, C.; Jiang, H.; Feng, J. Two-dimensional carbon allotrope with strong electronic anisotropy. *Phys. Rev. B* **2013**, *87*, 075453. [CrossRef]
61. Zhang, L.C.; Qin, G.; Fang, W.Z.; Cui, H.J.; Zheng, Q.R.; Yan, Q.B.; Su, G. Tinselenidene: A Two-dimensional Auxetic Material with Ultralow Lattice Thermal Conductivity and Ultrahigh Hole Mobility. *Sci. Rep.* **2016**, *6*, 19830. [CrossRef] [PubMed]